Photochemistry and Photobiology, 2020, 96: 692–698

Special Issue Research Article

Necrosis Depth and Photodynamic Threshold Dose with Redaporfin-PDT†

Luis B. Rocha[1], Helder T. Soares[1], Maria Inês P. Mendes[1], António Cabrita[2], Fábio A. Schaberle[1]* and Luís G. Arnaut[1]*

[1]Chemistry Department, University of Coimbra, Coimbra, Portugal
[2]Faculty of Medicine, University of Coimbra, Coimbra, Portugal

Received 28 November 2019, accepted 23 January 2020, DOI: 10.1111/php.13256

ABSTRACT

Predicting the extent of necrosis in photodynamic therapy (PDT) is critical to ensure that the whole tumor is treated but vital structures, such as major blood vessels in the vicinity of the tumor, are spared. The models developed for clinical planning rely on empirical parameters that change with the nature of the photosensitizer and the target tissue. This work presents an *in vivo* study of the necrosis in the livers of rats due to PDT with a bacteriochlorin photosensitizer named redaporfin using both frontal illumination and interstitial illumination. Various doses of light at 750 nm were delivered 15 min postintravenous administration of redaporfin. Sharp boundaries between necrotic and healthy tissues were found. Frontal illumination allowed for the determination of the photodynamic threshold dose—1.5×10^{19} photons cm^{-3}—which means that the regions of the tissues exposed to more than 11 mM of ROS evolved to necrosis. Interstitial illumination produced a necrotic radius of 0.7 cm for a light dose of 100 J cm^{-1} and a redaporfin dose of 0.75 mg kg^{-1}. The experimental data obtained can be used to inform and improve clinical planning with frontal and interstitial illumination protocols.

INTRODUCTION

Photodynamic therapy (PDT) combines light, photosensitizer molecules and molecular oxygen to generate reactive oxygen species (ROS) that, above a certain threshold, produce sufficient biological damage to trigger cell death (1,2). Although the oxidative stress produced by PDT may activate various cell death mechanisms (3), it is quite remarkable that PDT leads to a sharp boundary between a necrotic volume and the surrounding normal tissues. This motivated studies to assess threshold doses in terms of light fluence, photosensitizer concentration and its molar absorption coefficient, and establish the inherent sensitivity of tissues to ROS concentrations. The "photodynamic threshold dose" is defined as the number of photons absorbed by the photosensitizer per unit volume of tissue that produce tissue necrosis. Mathematically, it is expressed as $T_{th} = 2.3\varepsilon C_{loc} L_{th}$, where ε is the photosensitizer molar absorption coefficient at the treatment wavelength, C_{loc} is the tissue concentration of the photosensitizer and L_{th} is the light fluence (in J cm^{-2}) at the maximum depth (or radius) of necrosis (4). In this form, T_{th} is expressed in J cm^{-3} but can be readily converted to photons cm^{-3} using the wavelength of excitation. In these latter units, T_{th} measures the quanta of light absorbed by the photosensitizer that produces the biological endpoint. This quantity takes into account the wavelength of light, the local concentration of the photosensitizer and the corresponding light fluence needed to produce necrosis. In a sense, T_{th} is independent on the photosensitizer concentration in the tissue (5) because it compensates the drug dose with the light dose. It is assumed in this formulation that there should be a reciprocity between photosensitizer local concentration (C_{loc}) and light dose (L), as observed over a relatively wide range of doses in the early days of PDT (6), where photobleaching of the photosensitizer is neglected. However, this reciprocity can be expected to breakdown at low C_{loc} when the photosensitizer bleaching may become relevant, and at high C_{loc} when inner-filter effects or saturation of ROS may occur.

Studies on threshold doses signal the beginning of PDT dosimetry. Thomas Dougherty was also a precursor of PDT dosimetry with inspiring contributions on the combination of photosensitizer and light doses to determine thresholds of tissue necrosis and the limits that allow for normal tissue to fully recover after PDT (4). Our laboratory became involved in PDT in 1994, shortly after the first clinical approval of Photofrin (5). This approval triggered a tremendous enthusiasm throughout the world about the possibilities offered by PDT. We were deeply touched by this enthusiasm and started our research program guided by the seminal works of Dougherty. We aimed first at modeling the photophysical and photochemical properties of porphyrins, chlorins and bacteriochlorins, and then at the synthesis of new photosensitizers with properties designed for PDT (6). Our research efforts led to stable bacteriochlorins with low cytotoxicity that became very phototoxic under 750 nm light (7). One of these bacteriochlorins, named redaporfin, entered a clinical trial for advanced head and neck cancer (8). The adequacy of bacteriochlorins for PDT was noted very early on by Dougherty that emphasized their strong absorption maxima at very long wavelengths and their ability to generate singlet oxygen (9). In this work, we report photodynamic threshold doses with redaporfin.

*Corresponding authors emails: fschaberle@qui.uc.pt (Fábio A. Schaberle) and lgarnaut@ci.uc.pt (Luís Arnaut)
†This article is part of a Special Issue dedicated to Dr. Thomas Dougherty.

Many researchers employed healthy rat liver in threshold dose studies because its size, optical homogeneity and accessibility enable the establishment of extended dose-response relations (10–16). These studies revealed differences in T_{th} between various photosensitizers that cannot be assigned to differences in their spectroscopy or concentration in tissues, and that are significantly higher than their differences in singlet oxygen quantum yields. Moreover, T_{th} depends on the drug-to-light interval between the administration of the photosensitizer and the illumination of the target tissue. For example, T_{th} of Photofrin increases from 1.4×10^{18} to 3.4×10^{18} photons cm^{-3} at DLI = 10 min or 24 h, respectively (12). In view of the definition of T_{th}, this difference cannot be assigned to the decrease in photosensitizer concentration and should be related to the photodynamic sensitivity of the liver tissues when the photosensitizer is in the vascular compartment (DLI = 15 min) or in the cells (DLI = 24 h). In this example, the photodynamic sensitivity is higher for Photofrin in the vascular compartment. Although the healthy rat liver is not a realistic model of a tumor, quantities directly related to the photodynamic threshold dose, such as the PDT dose (17) and the singlet oxygen threshold dose (18–20), are currently used in dosimetry of tumors in animal models.

Light sources in PDT can be used in three different approaches: frontal, interstitial and endoluminal illumination. Frontal illumination is performed directing the beam of the light source to the surface of the target tissue, where most often a circular area is illuminated. Interstitial illumination and endoluminal illumination are performed using optical fibers with cylindrical light diffusion tips that deliver light perpendicular to the fiber, leading to a cylindrical illuminated volume (Fig. 1) (21). Consequently, the geometries of the illuminated volumes in the target tissues are very different. Frontal illumination can be recommended for the treatment of a large area and a limited depth, because the attenuation of light in tissues limits practical issue to PDT of lesions less than 2 cm in depth. Interstitial illumination inserting one or more optical fibers in the target tissue can be used in the treatment of deep-seated tumors as illustrated in Fig. 1 (22), but is more invasive. In endoluminal illumination, cylindrical diffusion tips are inserted in hollow cavities or ducts to treat lesions with cylindrical geometries, such as in esophageal and biliary tract lesions (23,24), and minimize invasiveness while allowing for the treatment of deep-seated tumors.

The prediction of the necrotic volume in frontal illumination critically depends on the depth (z) from the surface and that of interstitial/endoluminal illuminations depends of the radius (ρ) measured from the center of the optical fiber. Although many efforts have been made to predict light penetration in tissues and determine photodynamic threshold doses, physiological and physicochemical properties limit the accuracy of predictions (16,25,26), and necrotic volumes have to be determined experimentally for each photosensitizer to calibrate theoretical and computational models. The experimental data obtained in explicit dosimetry may later allow for predictions of clinical relevance (27). The ability to predict the extent of necrosis is of major importance in planning clinical procedures. For example, damage to critical structures such as blood vessels must be avoided, but, at the same time, the elimination of all neoplastic cells should be targeted to ensure a successful treatment (27).

This work reports the extent of necrosis resulting from redaporfin-PDT in rat liver using either frontal or interstitial illumination. The depth of necrosis z produced by frontal illumination and the radius of necrosis ρ measured after interstitial illumination were determined as a function of the light dose for a clinically relevant redaporfin dose. The extent of liver necrosis was assessed 72 h post-PDT by macroscopic measurements of z or ρ, and the boundaries between necrotic and viable tissue were confirmed by histology. The parameters obtained were used to estimate the photodynamic threshold dose in vascular PDT with redaporfin and to describe geometries of necrotic volumes.

MATERIALS AND METHODS

The study protocol was approved, as part of larger research project, by the local committee for animal welfare and the national veterinary agency with the reference number DGAV 0420/000/000/2011.

Nineteen female Wistars Han rats (Charles River Laboratories, Saint-Germain-sur-l'Arbresle, France) were used to test both frontal illumination and interstitial illumination. The animals were divided in seven treatment groups, four groups for frontal illumination (n = 1) and three groups for interstitial illumination (n = 3). One animal was used as non-treated control and was subjected to the photoactivation procedure with interstitial illumination but without receiving the redaporfin. The protocol was implemented when all the animals presented a body weight of at least 200 g. Throughout the study, the animals had free access to food and water. Redaporfin in a formulation containing Kolliphor® EL, ethanol and NaCl 0.9% was administered through the lateral tail vein to deliver a 0.75 mg kg^{-1} dose when the animals were under general anesthesia with i.p. injection of ketamine (75 mg kg^{-1}) and xylazine (10 mg kg^{-1}) mixture). Under aseptic conditions, a transversal incision was performed in the abdominal wall to expose part of the liver. The photoactivation of redaporfin with frontal or interstitial illumination was initiated 15 min after the administration of redaporfin.

Frontal illumination was performed using a light spot of 1 cm in diameter with a laser fluence rate of 130 mW cm^{-2}. Light doses of 10,

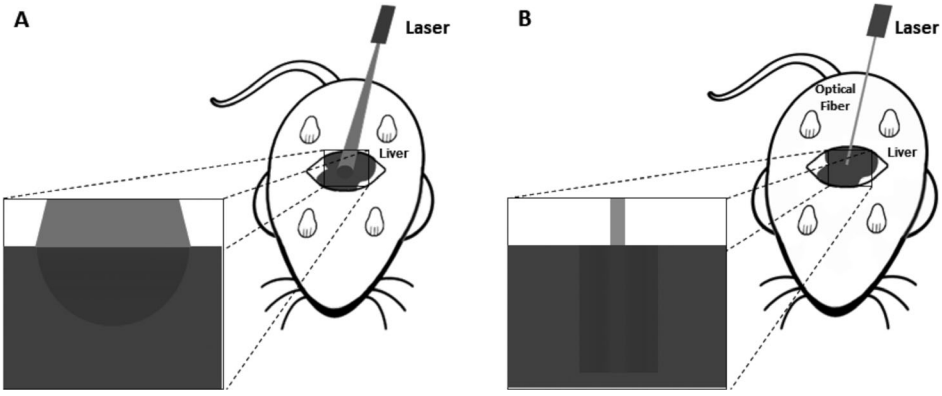

Figure 1. Schematic representation of frontal and interstitial illumination modalities often employed in PDT, where the expanded views are cross sections of the liver (A) along the axis of the frontal illumination laser beam or (B) along the fiber optic of the interstitial illumination.

25 and 50 J cm^{-2} ($n = 1$) were employed. Interstitial illumination was performed with the insertion of 1 cm of the cylindrical tip of an optical fiber in a path previously opened with a 21G needle into the liver tissue. Interstitial illumination employed light doses of 40, 100 and 150 J cm^{-1} ($n = 3$) at the diffusing fiber source strength of 150 mW cm^{-1}. Once the illumination was terminated, the transversal incision was closed in two planes, muscle and skin, with absorbable suture, and animal recovery was closely monitored. Analgesia was provided with subcutaneous administration of 2 mg kg^{-1} of butorphanol every 6 h for the first 48 h postsurgery. Following the recovery from the anesthesia, all animals resumed their normal activities.

Three days after the photoactivation of redaporfin, the animals were anesthetized with a ketamine (75 mg kg^{-1}) and xylazine (10 mg kg^{-1}) mixture via i.p. injection and then sacrificed by cervical dislocation. During the necropsy, the whole liver was removed and cut along a plane perpendicular to incidence plane (frontal) or to the path of optical fiber (interstitial) using a scalpel blade. The extent of necrosis in the liver was directly measured with a ruler and recorded in photographs.

Liver samples were fixed in formalin (10%) and processed in tissue processor Citadel 1000 from Shandon. Afterward, samples were embedded in paraffin and sectioned (4 mm) with a Shandon AS325 Retraction Microtome. Sections were stained with hematoxylin & eosin (H&E) and examined by a pathologist to evaluate the damage in the liver tissue. Redaporfin was kindly supplied by the Luzitin S.A. (Portugal).

RESULTS

Close monitoring of the animals in the 72 h postsurgical and illumination procedures revealed no visible signs of significant impact of the procedures on their normal health condition. Necropsy of each animal revealed that only the area of the liver where redaporfin was photoactivated presented a lesion and no other organ was affected. Necropsy of the nontreated control animal, submitted only to interstitial illumination with 150 J cm^{-1} without redaporfin, showed no sign of liver necrosis.

The liver tissue was evaluated 72 h after the PDT. Photographic records of the liver show very clearly a spot that corresponds to necrotic tissue (Fig. 2A–C). The boundary between necrotic and healthy liver tissue was confirmed by histological analysis (Fig. 3). A transversal slice in the center of the necrotic spot in the liver was made to measure the depth of necrosis and characterize the necrotic volume. The depth of necrosis z was measured relative to the center of the light spot. For instance, illumination with a light dose of 10 J cm^{-2} led to a necrosis depth of approximately 2.5 mm (Fig. 2B). The light dose of 50 J cm^{-2} lead to a necrosis depth that is larger than the thickness liver tissue in the direction of light propagation. Table 1 summarizes the results.

Interstitial illumination was performed inserting 1 cm of the cylindrical tip of the optical fiber, with 360° side emission (Fig. 1), into the liver tissue. In this case, the optical energy is delivered perpendicular to the fiber and along the radius ρ of the cylinder, and is given in Joule per centimeter. The cylindrical shape of the necrotic volume around the center of the lesions, where the tip was inserted, is shown in Fig. 4. The averages ($n = 3$ animals for each light dose) of necrotic radii are 3.8, 7.2 and 6.3 mm for the light doses of 40, 100 and 150 J cm^{-1}, respectively, Table 1. The control illuminated with 150 J cm^{-1} and no redaporfin is shown in Fig. 4 first row.

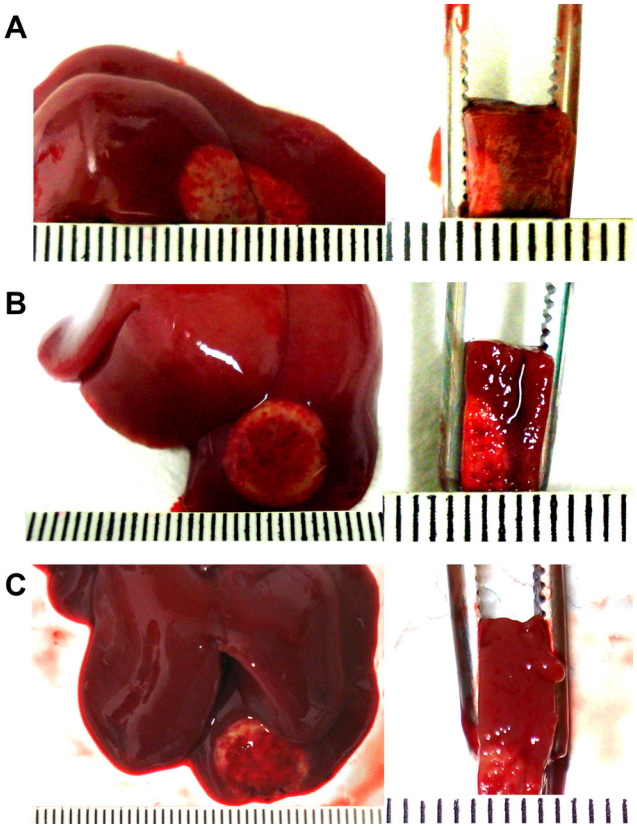

Figure 2. PDT of rat liver after frontal illumination for surface light fluences of (A) 5, (B) 10 and (C) 25 J cm^{-2}. The first column shows the liver after necropsy viewed from the perspective of the microlens at the tip of the optical fiber, where the discolored spots correspond to the illuminated area of 1 cm diameter. The second column shows the slices made to estimate the depth of necrosis, where the light was directed to the liver from left to right of each slice.

DISCUSSION

Table 1 summarizes the data pertinent for the relation between light dose and the extent of necrosis in frontal and interstitial illuminations. Although the liver of rats is a relatively large organ, it was only possible to assess the necrosis depth for doses below 25 J cm^{-2} in frontal illumination. The light dose of 50 J cm^{-2} exceeded the thickness of the liver in the direction of propagation of light. It is interesting to compare these results with those reported in earlier determinations of photodynamic threshold doses using vascular PDT (drug-to-light intervals in the 10–15 min range) with other photosensitizers. For example, administration of 10 mg kg^{-1} of Photofrin followed by the delivery of 90 J cm^{-2} at 630 nm led to a liver necrosis depth of approximately 3 mm (5), whereas 0.75 mg kg^{-1} of redaporfin with 25 J cm^{-2} at 750 nm led to a necrosis depth of approximately 4 mm. Redaporfin produces a significantly deeper necrosis at a drug-light combination approximately 50 times lower than that of Photofrin. This is certainly related to the 100 times higher ε of redaporfin relative to Photofrin (7) and to the higher light fluences in the tissues enabled by the higher optical penetration depth of 750 *versus* 630 nm light. Both ε and local light fluence are taken into account in the photodynamic threshold dose. Hence, if these parameters are properly accounted, the photodynamic threshold dose should be similar for redaporfin and Photofrin even though redaporfin is much more potent than Photofrin.

The macroscopic evaluation of the transition between necrotic and healthy liver tissue corresponded well with the histology of the tissue samples. The illumination of the liver was always

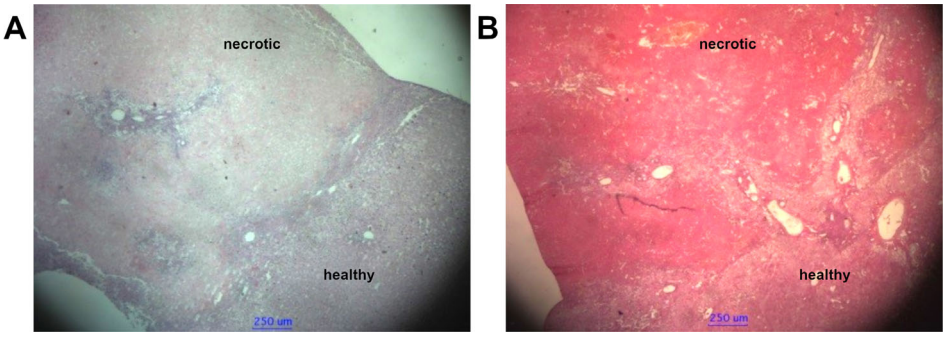

Figure 3. Typical histological images showing the transition between necrotic and healthy liver tissue. (A) Frontal illumination with 25 J cm^{-2}. (B) Interstitial illumination with 150 J cm^{-2}.

Table 1. Light dose and extent of necrosis determined for frontal (n = 1) and interstitial (n = 3) illumination in vascular PDT with 0.75 mg kg^{-1} of redaporfin (average ± STD).

Frontal illumination		Interstitial illumination		
Light dose* J cm^{-2}	z mm	Light dose† J cm^{-1}	ρ mm	Average mm
5	1.6	40	4.0 4.0 3.5	3.8 ± 0.4
10	2.5	100	8.0 7.0 6.5	7.2 ± 0.8
25	≈4	150	5.5 7.0 6.5	6.3 ± 0.8
50	>4	Control (150)	0	0

*Fluence at the surface of the tissue. †Optical energy released per unit length of the diffusing optical fiber.

performed 15 min after the intravenous administration of 0.75 mg kg^{-1} of redaporfin, when this photosensitizer is almost entirely confined to the vascular compartment. Hemorrhagic necrosis was found at higher amplifications of the histological sections, together with inflammatory infiltrates.

The depth of necrosis can be expressed as (28)

$$z_{max} = \delta \ln(k_s L_0 / L_{th})$$

where the backscatter factor k_s accounts for light reflected from underlying tissue, which makes the fluence just below the surface of the tissue higher than the in-air fluence L_0. We use this expression to calculate δ (effective optical penetration depth for which light attenuates to $1/e$) and L_{th} using the necrosis depths experimentally obtained for various surface light doses (L_0) (29,30). The use of this equation requires an estimate for k_s for normal rat liver irradiated at 750 nm.

The optical properties of normal rat liver were reported for irradiation at 615, 640 and 665 nm (31). The optical penetration depths are 0.081, 0.106 and 0.125 cm, respectively. In particular, the optical absorption coefficient and the reduced scattering coefficient at 665 nm are μ_a = 0.18 mm^{-1} and μ_s' = 1.17 mm^{-1}, respectively (31). Using the analytical expression (32) for backscatter of broad beams as a function of the diffuse reflectance and the dependence of the diffuse reflectance on the optical properties μ_a and μ_s', we calculate k_s = 4.0 at 665 nm. The value at 750 nm should be slightly lower. We employed k_s = 3.8.

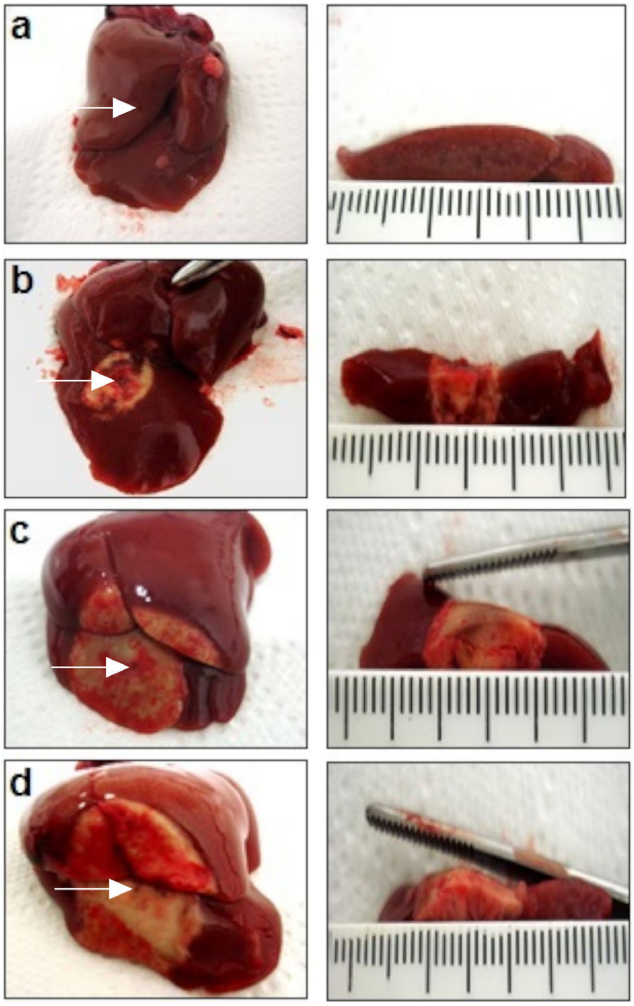

Figure 4. PDT of rat liver with interstitial illumination where the left column shows the liver after necropsy (the arrowhead indicates the insertion point of the cylindrical diffuser) and the right column shows the transversal slices used to measure the radius of necrosis from the fiber insertion axis with light doses, from top to bottom rows, of 150 (control, without redaporfin), 40, 100 and 150 J cm^{-1}.

Figure 5 shows that the logarithmic dependence of z_{max} on L_0 is followed at least up to 25 J cm^{-2} and allows for the calculation of δ = 0.15 cm and L_{th} = 6.8 J cm^{-2}. This estimate of L_{th} includes a backscatter factor k_s = 3.8. The value of δ at 750 nm

is consistent with the known increase of δ when the wavelength increases from the red to the near-infrared (33). In the conditions of Fig. 5, we estimate that a light dose of 50 J cm^{-2} leads to z_{max} = 0.5 cm for a wide illumination filed (>4 cm in diameter).

It must be emphasized that, for identical incident fluence, a beam with larger diameter results in a higher fluence in the volume where light propagation in tissue is in the so-called diffusion region (34). We employed an incident beam diameter of 1 cm in frontal illumination and its effect in the shape of the necrotic volume is represented in Fig. 6. A beam with larger diameter is expected to produce a larger depth of necrosis for the higher incident fluences employed in this work.

The determination of the photodynamic threshold dose requires an estimate of C_{loc} in the tumor. We use the ratio of redaporfin concentrations in the liver and blood of mice at DLI = 15 min (liver/blood = 0.44) (35) and the fact that the volume of plasma is approximately 65% of that of blood, to estimate the ratio liver/plasma = 0.29. This, together with plasma concentration of redaporfin in rats for the same DLI ($\approx$60 μg mL^{-1} for a i.v. administration of 6 mg kg^{-1} (36)), leads to the redaporfin concentration in the liver of 2.15 μg mL^{-1} scaled for the administration of 0.75 mg kg^{-1} of redaporfin used in this work. The use of redaporfin molecular weight, 1135 g mol^{-1}, allows for the estimate $C_{loc} \approx 2$ μM in the rat liver. Given ε_{750} = 125 000 M^{-1} cm^{-1} for redaporfin in tissues (37), we estimate T_{th} = 3.8 J cm^{-3}, or 1.5 × 10^{19} photons cm^{-3} when the conversion factor for 750 nm is employed (hc/λ = 2.65 × 10^{-19} J). These estimates are based on L_{th} with the backscatter factor. This is in good agreement with photodynamic threshold doses reported for other photosensitizers (12). In particular, the photodynamic threshold doses of Photofrin, monosulfonated aluminum chlorophthalocyanine and its tri/tetrasulfonated analogue are 1.4 × 10^{18}, 1.6 × 10^{18} and 2.3 × 10^{19} photons cm^{-3}, respectively, when liver illumination is made 10 min postinjection.

It is of interest to calculate the concentration of ROS necessary to produce necrosis (28)

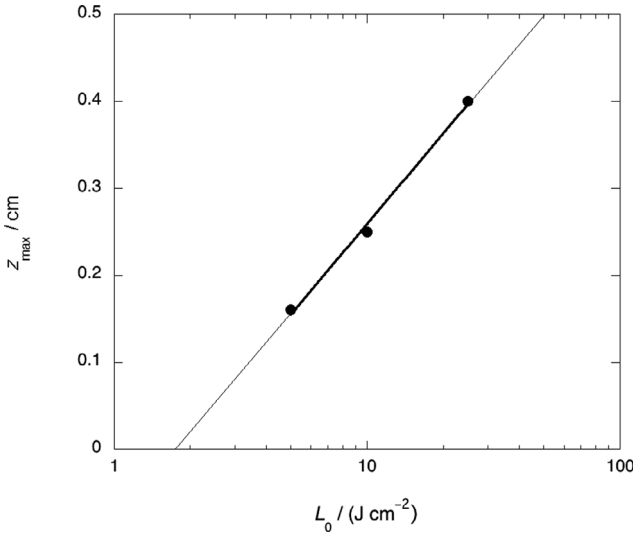

Figure 5. Dependence of the depth of rat liver necrosis on the surface light fluence for vascular PDT with 0.75 mg kg^{-1} of redaporfin and an illumination area with 1 cm^2 in diameter. The value of L_{th} is given by the x-intercept (1.8 J cm^{-2}) multiplied by the backscatter factor (k_s = 3.8 at 750 nm).

$$[\mathrm{ROS}] = bT_{th}\Phi_{ROS}f$$

where $b = \lambda/(hcN_A) = 6.26 \times 10^{-6}$ is the number of moles of photons per J for light at 750 nm and Φ_{ROS} is the ROS quantum yield (Φ_{ROS} = 0.59 for redaporfin (7)) and f the fraction of ROS that attack sensitive targets in the tissue. The expression above must be multiplied by 1000 when T_{th} is expressed in J cm^{-3}. We obtain [ROS] = 11 mM when $k_s f = 3$, in very good agreement with other estimates (28). The backscatter was included in T_{th} (k_s = 3.8), and the faction of ROS reacting with sensitive targets is assumed to be f = 0.8. The concentration of ROS that produces necrosis in redaporfin-PDT can be compared with the reacted ROS concentration $[ROS]_{rx}$ developed in other dosimetry models to predict the cure index after vascular PDT of murine tumors (38). $[ROS]_{rx}$ was determined for Visudyne® and for Tookad®-soluble at using DLI = 15 min, and values of 0.23 mM (38) and 21 mM (39) were obtained, respectively, which bracket the [ROS] determined for redaporfin.

Interstitial illumination with 0.75 mg kg^{-1} of redaporfin and 100 J cm^{-1} achieved a necrotic radius $\rho \approx 0.7$ cm which compares well with other photosensitizers (40). For 1 cm length cylindrical diffusion, this corresponds to a necrotic volume of 1.5 cm^3 in the liver. The necrotic volume obtained with interstitial illumination in this work is higher than with frontal illumination in spite of the stronger geometrical dilution of the radiant

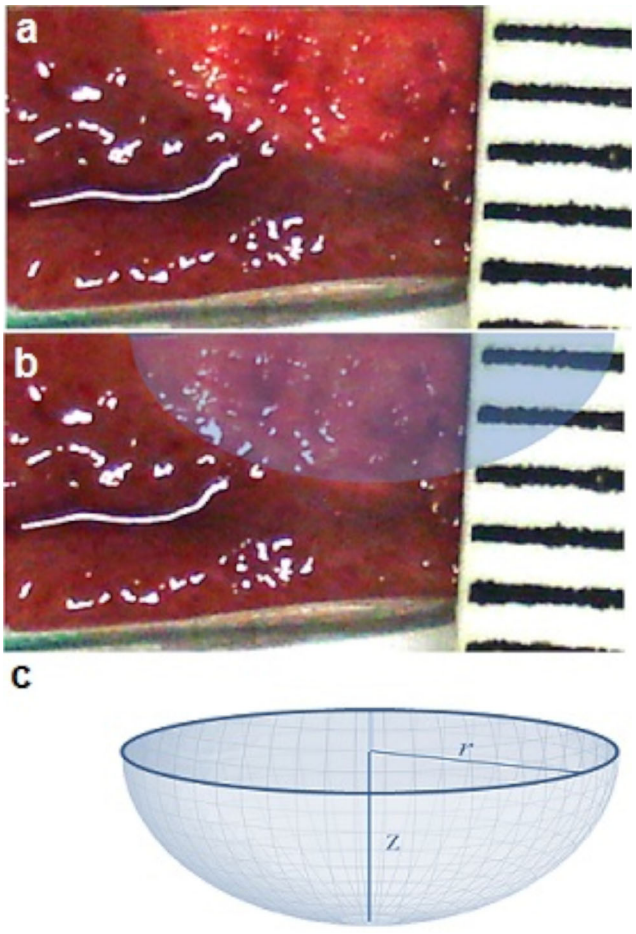

Figure 6. Modeling of necrosis in frontal illumination for incident beam diameter of 1 cm and fluence of 10 J cm^{-2} showing that the necrotic volume takes an ellipsoidal shape with $z_{max} \approx 2$ mm.

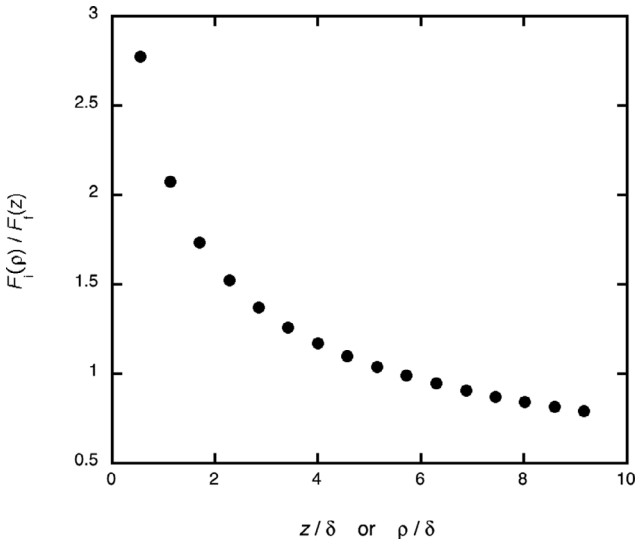

Figure 7. Ratio of fluence rates in interstitial and frontal illuminations as a function of the reduced distance (ρ/δ) or (z/δ).

power. However, the comparison between the two protocols must take into consideration the differences between the light doses delivered. Such differences are better understood in terms of fluence rates.

The fluence rate for frontal illumination is described by

$$F_f(z) = F_{f0} k_s \exp(-z/\delta)/(2\mu_a\delta).$$

and for a cylindrical diffuser, it can be approximated as

$$F_i(\rho) = F_{i0} k_s' K_0(\rho/\delta)/(2\pi\mu_a\delta^2)$$

where F_{f0} is the fluence rate at the source (frontal illumination, W cm^{-2}), F_{i0} is the diffusing fiber source strength (interstitial illumination, W cm^{-1}), μ_a is the absorption coefficient (in cm^{-1}) and $K_0(\rho/\delta)$ is the zeroth-order modified Bessel function (41). These expressions include backscatter factors, k_s and k_s', which are mostly relevant within a few mm of the tissue surface. These backscatters tend to cancel each other when ratio of these fluence rates is computed as

$$F_i(\rho)/F_f(z) = F_{i0} K_0(\rho/\delta)/[F_{f0}\pi\delta\exp(-z/\delta)].$$

Figure 7 presents this ratio using the fluence rates at source of this work (F_{f0} = 0.166 W cm^{-2} and F_{i0} = 0.150 W cm^{-1}) and the value of δ determined for liver (δ = 0.15 cm). The ratio becomes unity at $\rho \approx 1$ cm and then $F_i(\rho)$ becomes smaller than $F_f(z)$ because of its stronger geometrical dilution.

It is somewhat surprising to realize that light doses higher than 100 J cm^{-1} did not increase the necrotic volume in interstitial illumination. Its stronger dependence on the distance requires a steeper increase in light doses to extend the necrotic volume. This limitation can be overcome with the insertion of multiple fibers. It also comes with the advantage of a potentially sharper threshold than in frontal illumination because the fluence rate has a stronger dependence of distance in this case.

CONCLUSIONS

The rat liver is a good model to investigate the depth of necrosis produced in PDT protocols because it allows for the study of depths up to 5 mm and can be used to compare data reported for different photosensitizers. The data obtained are relevant for explicit dosimetry and can inform models used in the planning of clinical procedures. We showed that redaporfin-PDT at DLI = 15 min (vascular PDT) leads to sharp transitions between necrotic and healthy tissue, both in frontal and interstitial protocols. These results further corroborate the usefulness of the "photodynamic threshold dose," that was determined as 1.5 × 10^{19} photons cm^{-3}, in good agreement with the literature data on widely different photosensitizers and drug-to-light intervals. This dose roughly corresponds to 11 mM of ROS, which seem to be the oxidative stress required to produce rat liver necrosis. The similar photodynamic threshold doses obtained for different photosensitizers mean that their ability to produce necrosis is directly proportional to their concentration in the target tissue, to their molar absorption coefficient and to the light fluence in the tissues. The tissue concentrations of the photosensitizers in vascular PDT depend essentially on the dose employed in the intravenous administration. Hence, in vascular PDT, where the supply of molecular oxygen is not a limiting factor, the relative potency of the photosensitizers is determined by ε and by L_{th}, which favor photosensitizers with strong absorbances in the near-infrared. This analysis neglects the photobleaching of the photosensitizers, which does not seem to play an important role for redaporfin in the conditions employed in this study. A more exact analysis should also take into account the quantum yield for the generation of ROS; nevertheless, the concept of "photodynamic threshold dose" remains very useful today.

Dougherty emphasized the important of proper dosing very early in the development of PDT. It is a pleasure and an honor to contribute with this first approach to redaporfin-PDT dosing to the Thomas Dougherty memorial issue in *Photochemistry and Photobiology*.

Acknowledgements—This work was supported by the Portuguese Science Foundation and QREN/FEDER (UID/QUI/00313/2019, PTDC/QEQ-MED/3521/2014) LaserLab Portugal (022124) and by H2020 Research Infrastructures (LaserLab Europe 654148). FS thanks POCI-01-0145-FEDER-027996 for a grant. HT and MIM thank FCT for PhD grants SFRH/BD/119058/2016 and PD/BD/143129/2019, respectively. We thank Eduardo Costa and Ana Rute Duarte for technical support in sample preparation for histology.

REFERENCES

1. Dougherty, T. J., C. J. Gomer, B. W. Henderson, G. Jori, D. Kessel, M. Korbelik, J. Moan and Q. Peng (1998) Photodynamic therapy. *J. Natl. Cancer Inst.* **90**, 889–905.
2. Dabrowski, J. M. and L. G. Arnaut (2015) Photodynamic therapy (PDT) of cancer: From a local to a systemic treatment. *Photochem. Photobiol. Sci.* **14**, 1765–1780.
3. Donohoe, C., M. O. Senge, L. G. Arnaut and L. C. Gomes-da-Silva (2019) Cell death in photodynamic therapy: From oxidative stress to anti-tumor immunity. *BBA Rev. Cancer* **1872**, 188308.
4. Potter, W. R., T. S. Mang and T. J. Dougherty (1987) The theory of photodynamic therapy dosimetry: Consequences of photodestruction of sensitizer. *Photochem. Photobiol.* **46**, 97–101.
5. Dougherty, T. J. (1993) Photodynamic therapy. *Photochem. Photobiol.* **58**, 895–900.
6. Arnaut, L. G. (2011) Design of porphyrin-based photosensitizers for photodynamic therapy. *Adv. Inorg. Chem.* **63**, 187–233.
7. Arnaut, L. G., M. M. Pereira, J. M. Dąbrowski, E. F. F. Silva, F. A. Schaberle, A. R. Abreu, L. B. Rocha, M. M. Barsan, K. Urbańska, G. Stochel and C. M. A. Brett (2014) Photodynamic therapy efficacy enhanced by dynamics: the role of charge transfer and photostability in the selection of photosensitizers. *Chem. Eur. J.* **20**, 5346–5357.

8. Santos, L. L., J. Oliveira, E. Monteiro, J. Santos and C. Sarmento (2018) Treatment of head and neck cancer with photodynamic therapy with redaporfin: A clinical case report. *Case Rep. Oncol.* **11**, 769–776.
9. MacDonald, I. J. and T. J. Dougherty (2001) Basic principles of photodynamic therapy. *J. Porphyrins Phthalocyanines* **5**, 105–129.
10. Bown, S. G., C. J. Tralau, P. D. Smith, D. Akdemir and T. J. Wieman (1986) Photodynamic therapy with porphyrin and phthalocyanine sensitisation: Quantitative studies in normal rat liver. *Br. J. Cancer* **54**, 43–52.
11. Farrell, T. J., B. C. Wilson, M. S. Patterson and R. Chow (1991) The dependence of photodynamic threshold dose on treatment parameters in normal rat liver in vivo. *Proc. SPIE* **1426**, 146–155.
12. Farrell, T. J., B. C. Wilson, M. S. Patterson and M. C. Olivo (1998) Comparison of the in vivo photodynamic threshold dose for Photofrin, mono- and tetrasulfonated aluminum phthalocyanine using a rat liver model. *Photochem. Photobiol.* **68**, 394–399.
13. Woodhams, J. H., L. Kunz, S. G. Bown and A. J. MacRobert (2004) Correlation of real-time haemoglobin oxygen saturation monitoring during photodynamic therapy with microvascular effects and tissue necrosis in normal rat liver. *Br. J. Cancer* **91**, 788–794.
14. Ferreira, J. et al (2007) Experimental determination of threshold dose in photodynamic therapy in normal rat liver. *Laser Phys. Lett.* **4**, 469–475.
15. Rego, R. F. et al (2013) In vivo study of necrosis on the liver tissue of Wistar rats: a combination of photodynamic therapy and carbon dioxide laser ablation. *Laser Phys.* **23**, 075603.
16. Kareliotis, G., M. Papachristou, D. Priftakis, I. Datseris and M. Makropoulou (2019) Computational study of necrotic areas in rat liver tissue treated with photodynamic therapy. *J. Photochem. Photobiol. B* **192**, 40–48.
17. Rizvi, I., S. Anbil, N. Alagic, J. P. Celli, L. Z. Zheng, A. Palanisami, M. D. Glidden, B. W. Pogue and T. Hasan (2013) PDT dose parameters impact tumoricidal durability and cell death pathways in a 3D ovarian cancer model. *Photochem. Photobiol.* **89**, 942–952.
18. Wang, K. K.-H., J. C. Finlay, T. M. Busch, S. M. Hahn and T. C. Zhu (2010) Explicit dosimetry for photodynamic therapy: macroscopic singlet oxygen modeling. *J. Biophoton.* **3**, 304–318.
19. Penjweini, R., B. Liu, M. M. Kim and T. C. Zhu (2015) Explicit dosimetry for 2-(1-hexyloxyethyl)-2-devinyl pyropheophorbide-a-mediated photodynamic therapy: macroscopic singlet oxygen modeling. *J. Biomed. Opt.* **20**, 128003.
20. Qiu, H., M. M. Kim, R. Penjweini, J. C. Finlay, T. M. Busch, T. Wang, W. Guo, K. A. Cengel, C. B. Simone, E. Glatstein and T. C. Zhu (2017) A comparison of dose metrics to predict local tumor control for Photofrin-mediated photodynamic therapy. *Photochem. Photobiol.* **93**, 1115–1122.
21. Mang, S. T. (2004) Lasers and light sources for PDT: past, present and future. *Photodiagnosis Photodyn. Ther.* **1**, 43–48.
22. Shafirstein, G., D. A. Bellnier, E. Oakley, S. Hamilton, M. Habitzruther, L. Tworek, A. Hutson, J. A. Spernyak, S. Sexton, L. Curtin, S. G. Turowski, H. Arshad and B. Henderson (2018) Irradiance controls photodynamic efficacy and tissue heating in experimental tumours: implication for interstitial PDT of locally advanced cancer. *Br. J. Cancer* **119**, 1191–1199.
23. Moghissi, K. and K. Dixon (2003) Photodynamic therapy (PDT) in esophageal cancer: a surgical view of its indications based on 14 years experience. *Technol. Cancer Res Treat.* **2**, 319–326.
24. Shim, C., Y. Cheon, S. Cha, S. Bhandari, J. Moon, Y. Cho, Y. Kim, L. Lee, M. Lee and B. Kim (2005) Prospective study of the effectiveness of percutaneous transhepatic photodynamic therapy for advanced bile duct cancer and the role of intraductal ultra-sonography in response assessment. *Endoscopy* **37**, 425–433.
25. Wang, K. K.-H., S. Mitra and T. H. Foster (2008) Photodynamic dose does not correlate with long-term tumor response to mTHPC-PDT performed at several drug-light intervals. *Med. Phys.* **35**, 3518–3526.
26. Sandell, J. L. and T. C. Zhu (2011) A review of in-vivo optical properties of human tissues and its impact on PDT. *J. Biophotonics* **4**, 773–787.
27. Pogue, B. W., J. T. Elliott, S. C. Kanick, S. C. Davis, K. S. Samkoe, E. V. Maytin, S. P. Pereira and T. Hasan (2016) Revisiting photodynamic therapy dosimetry: reductionist & surrogate approaches to facilitate clinical success. *Phys. Med. Biol.* **61**, R57–89.
28. Photodynamic Therapy Dosimetry, (American Association of Physicists in Medicine, 2005).
29. van Gemet, J. C., M. C. Berenbaum and G. H. M. Gijsbers (1985) Wavelength and ligh-dose dependence in tumour phototherapy with haematoporphyrin derivative. *Br. J. Cancer* **52**, 43–49.
30. Ferraz, R. C. M. C., J. Ferreira, P. F. C. Menezes, C. H. Sibata, O. C. e Silva and V. S. Bagnato (2009) Determination of threshold dose of photodynamic therapy to measure superficial necrosis. *Photomed. Laser Surg.* **27**, 93–99.
31. Patterson, M. S., B. C. Wilson and R. Graff (1990) In vivo tests of the concept of photodynamic threshold dose in normal rat liver photosensitized by aluminum chlorosulphonated phthalocyanines. *Photochem. Photobiol.* **51**, 343–349.
32. Ong, Y. H. and T. C. Zhu (2016) Analytic function for predicting light fluence rate of circular fields on a semi-infinite turbid medium. *Opt. Exp.* **24**, 26261–26281.
33. Bashkatov, A. N., E. A. Genina, V. I. Kochubey and V. V. Tuchin (2005) Optical properties of human skin, subcutaneous and mucous tissues in the wavelength range from 400 to 2000 nm. *J. Phys. D: Appl. Phys.* **38**, 2543–2555.
34. Chen, Q., B. C. Wilson, M. O. Dereski, M. S. Patterson, M. Chopp and F. W. Hetzel (1992) Effects of light beam size on fluence distribution and depth of necrosis in seperficially applied photodynamic therapy of normal rat brain. *Photochem. Photobiol.* **56**, 379–384.
35. Saavedra, R., L. B. Rocha, J. M. Dabrowski and L. G. Arnaut (2014) Modulation of biodistribution, pharmacokinetics, and photosensitivity with the delivery vehicle of a bacteriochlorin photosensitizer for photodynamic therapy. *ChemMedChem* **9**, 390–398.
36. Sa, L.LUZ11: Single Intravenous Dose Pharmacokinetic Study in the Male and Female Sprague Dawley Rat, (internal report, 2012).
37. Rocha, L. B., L. C. Gomes-da-Silva, J. M. Dabrowski and L. G. Arnaut (2015) Elimination of primary tumours and control of metastasis with rationally designed bacteriochlorin photodynamic therapy regimens. *Eur. J. Cancer* **51**, 1822–1830.
38. Sheng, T., Y. H. Ong, T. M. Busch and T. C. Zhu (2019) Reactive oxygen species explicit dosimetry to predict tumor growth for BPD-mediated vascular photodynamic therapy. *Proc. SPIE* **10861**, 108610A.
39. Ong, Y. H., M. M. Kim, Z. Huang and T. C. Zhu (2018) Reactive oxygen species explicit dosimetry (ROSED) of a type 1 photosensitizer. *Proc. SPIE* **10476**, 104760V.
40. Martin, N. E. and S. M. Hahn (2004) Interstitial photodynamic therapy for prostate cancer: a developing modality. *Photodiagnosis Photodynamic Ther.* **1**, 123–136.
41. Jacques, S. L. (1998) Light distributions from point, line and plane sources for photochemical reactions and fluorescence in turbid biological tissues. *Photochem. Photobiol.* **67**, 23–32.